The evolution of aerosols mixing state derived from a field campaign in Beijing: implications to the particles aging time scale in urban atmosphere

Jieyao Liu[1], Fang Zhang[2], Jingye Ren[3], Lu Chen[4], Anran Zhang[2], Zhe Wang[2], Songjian Zou[2], Honghao Xu[2], Xingyan Yue[1]

[1] School of Geographical Sciences, Hebei Normal University, Shijiazhuang, China

[2] School of Civil and Environmental Engineering, Harbin Institute of Technology (Shenzhen), Shenzhen, China

[3] Xi'an Institute for Innovative Earth Environment Research, Xi'an, China

[4] Faculty of Geographical Science, Beijing Normal University, Beijing, China

Correspondence to: Fang Zhang (zhangfang2021@hit.edu.cn)

Abstract

The mixing states and aging time scale of aerosol particles play a vital role in evaluating their climate effects. Here, by using the field measurement at a site of the urban Beijing, we have identified four different real-time mixing patterns of size-resolved particles, which are defined as less hygroscopic (LH) internally-mixed, externally-mixed, transitional externally-mixed and more hygroscopic (MH) internally-mixed particles, with atmospheric fraction of 0-10%, 20-46%, 17-24% and 27-56% respectively. The fraction depends on particles size, with the maximum fraction of MH internally-mixed particles at 80 and 110 nm, and the minimum fraction of LH internally-mixed particles across all sizes, implying rapid mixing and aging of ambient particles during the observational period. The diurnal variations of the mixing states of particles in all sizes investigated (40, 80, 110, 150 and 200 nm) present an apparent aging process from externally-mixed to MH internally-mixed, which typically spans

a duration of approximately 5–10 hours from 8:00–10:00 to 15:00–17:00, revealing the mixing (aging) timescale of aerosols in polluted urban atmosphere. Additionally, our results suggest that those fine aerosol particles experience aging through both the photochemical process and non-photochemical growth during the campaign. Furthermore, through a comprehensive review of the mixing/aging timescale of particles adopted in current models and derived from observations, we show the great discrepancy between observations and models, highlighting the importance to parameterize their aging time scale based on more field campaigns.

1 Introduction

The mixing state of atmospheric aerosol particles can affect the hygroscopicity and the ability to serve as cloud condensation nuclei (CCN), and thus the air quality and climate (Müller et al., 2017; Xu et al., 2021; Yao et al., 2022; Ge et al., 2024). It has been shown that the aerosol mixing state is closely related to the hygroscopicity (Chen et al., 2022; Fan et al., 2020). Ren et al. (2018) predicted the concentration of CCN using five different mixing state schemes and found that the influence of aerosol mixing state on its activation characteristics ranged from –34% to +16%. Neglecting particle mixing structure can also lead to significant overestimation of the aerosol absorption efficiency (Yao et al., 2022). Therefore, it is important to account for the information of mixing state of ambient particles in climate models so as to reduce the uncertainty in evaluating their environmental and climate effects.

The mixing states of ambient particles are complex. Particles in areas affected by primary emissions are mainly ~~with~~ in an external mixing state (i.e., the chemical components of particles exist independently), while aerosols in relatively clean areas are mainly transported from elsewhere and have a higher degree of internal mixing (Swietlicki et al.,

2008; Enroth et al., 2018; Chen et al., 2022). Internal mixing typically includes uniform composition or core–shell structures (Jacobson et al., 2001). The former refers to the same proportion of species in any part of the aerosol component, while the latter is defined as the mixing state formed by certain chemical components coating or condensing on the surface of other components during the aging process. Also, the mixing state of aerosol particles is variable. Freshly emitted particles undergo various processes, including photochemical and aqueous-phase processes, as well as physical processes such as coagulation and condensation, leading to an increase in their degree of internal mixing. This gradual transition from external to internal mixing characterizes the aging process of particles. The aging timescale varies greatly between clean and polluted areas (Peng et al., 2016; Chen et al., 2017; Ghosh et al., 2021). However, the timescale of aging process of particles was commonly fixed in many models and did not depend on environmental conditions (Chen et al., 2017; Ghosh et al., 2021), which may introduce great uncertainty in the prediction of regional aerosol concentration and the evaluation of aerosol climate effects (Ghosh et al., 2021). Therefore, capturing the temporal scales of the evolution of the aerosol mixing state based on field campaigns is crucial for accurately parameterizing the aging timescale of aerosol particles in models, thereby enhancing the precision of simulations pertaining to the environmental and climatic impacts of aerosols.

At present, some studies have characterized the mixing state and aging process of black carbon (BC) aerosols using different instruments. Transmission electron microscopy (TEM) has been used to determine the mixing state of individual particles in China (Li et al., 2016; Zhang et al., 2023). However, based on TEM technique, a large number of aerosol samples

are required so as to make the results statistically significant~~with the significance of statistics~~, which means a high cost both on labors and materials. The most important issue is that the mixing state of particles may change during collection and transportation. Recently, aerosol time-of-flight mass spectrometry (ATOFMAS) and soot-particle aerosol mass spectrometry (SP-AMS) have been used to measure the mixing state of BC and coated aerosol species in real time (Liu et al., 2019; Xie et al., 2020). Overall, previous studies focused more on the mixing state of BC of single-particles (Saha et al., 2018; Xie et al., 2020; Chen et al., 2020). ~~While~~However, the mixing state of particles across a population in ambient atmosphere is more complex (Riemer et al., 2019). According to Winkler's definition, the "internal mixing" means when all particles within the bulk aerosol populations ~~are with~~have the same compositions. ~~While, t~~The "external mixing" means when all particles consist of pure species and have distinct compositions (Winkler et al., 1973; Riemer et al., 2019). Note that in Riemer et al. (2019), the definition refers to the bulk not the sized-resolved mixing state of aerosol particles. In this study, the size resolved mixing state of aerosol particles has been identified according to the patterns of the probability density function of hygroscopic growth factor/hygroscopic parameter (κ) (Gf-PDF; κ-PDF) measured using a humidity tandem differential mobility analyzer (H-TDMA) (Hong et al., 2018; Shi et al., 2022; Spitieri et al., 2023). For example, the internally-mixed aerosol populations with diameter of 40 nm are characterized by the single hygroscopic mode of Gf-PDF/κ-PDF, while the externally-mixed particles have bi- or trimodal distributions of Gf-PDF/κ-PDF. However, most studies based on the H-TDMA measurements only made qualitative descriptions of the particle mixing state when explaining the variations in the aerosol hygroscopicity (Wang et al., 2019; Chen et al.,

2022; Shi et al., 2022).

In this study, with the aim of obtaining insights into the mixing state and mixing (aging) time scale of ambient particles in urban area, we have identified four different types of size-resolved particles mixing states, and characterized their real-time variations using the field measured hygroscopic growth factor by the H-TDMA in urban Beijing. The evolution of mixing state of particles with specific sizes was explored to imply the mixing (aging) timescale of their aging from the diurnal variations during clear and cloudy days. Finally, we compared the mixing/aging timescale of aerosol particles with that adopted in current models and other field observations reported in previous literatures.

2 Methods

The campaign was conducted at the meteorological tower branch of the Institute of Atmospheric Physics (IAP), Chinese Academy of Sciences to measure the physical and chemical properties of particles and the meteorological conditions from 19 May to 18 June 2017 in Beijing. The instruments used in this study were deployed in a container at ground (the sampling inlet is located at ~8 m on the meteorological tower). The hygroscopicity of aerosols with different dry sizes (40, 80, 110, 150 and 200 nm) and particle number distribution in the size range of 10–550 nm was measured using a H-TDMA and a Scanning Mobility Particle Sizer (SMPS), respectively. The mass concentration of the non-refractory chemical compositions in particulate matter with diameter < 1 μm (PM_1) was measured by an Aerodyne high-resolution time-of-flight aerosol mass spectrometer (HR-ToF-AMS) (Xu et al., 2019), and the BC was measured by a 7-wavelength aethalometer (AE33, Magee Scientific Corp). More details about the sites, instruments and calibrations can be found in previous literatures (Zhang et al., 2017; Wang et al., 2019; Fan et al., 2020; Chen et al., 2022). Since the campaign site was located at the urban area of Beijing, where the atmospheric fine

aerosols are more frequently affected by local traffic and cooking sources (Sun et al., 2015). In addition, during the observation period of summertime, the site was predominately affected by the warm and humid southeastern air parcels (~~Figure~~ Fig. S1); while the dust events normally originate from northwestern regions occurring in springtime (Li et al., 2020) and typically with particle sizes in coarse mode (Wang et al., 2023). Therefore, the contribution from dust aerosols could be negligible in this study.

Here, we mainly describe the interpretation criteria for the mixing state of particles. The Gf-PDF was obtained by $TDMA_{inv}$ algorithm in this study (Gysel et al., 2009). Then, the κ-PDF of size-resolved particles was retrieved according to the κ-Köhler theory (Petters and Kreidenweis, 2007). Subsequently, we accurately defined four mixing states based on the κ-PDF patterns and the number of peaks in κ-PDF (~~Figure~~ Fig. 1, ~~Figure~~ Fig. S2). The κ-PDF of type 1 exhibits bimodal distributions with a much higher proportion (> 70%) of hydrophobic mode or less hygroscopic mode (LH; the peak of κ-PDF occurs at $\kappa < 0.1$), was thus defined as LH internally-mixed state (type 1). Mixing type 2 (Externally-mixed) is characterized by bimodal distributions in the κ-PDF for both LH and more hygroscopic (MH, $\kappa \geq 0.1$) modes, with less than 30% difference in the fraction of the two modes. ~~Mixing type 2 refers to that the κ-PDF exhibits bimodal distributions in both LH and more hygroscopic (MH, $\kappa \geq 0.1$) modes, with the difference of less than 30% between the fraction of the two modes.~~ The κ-PDF pattern with trimodal distributions was named as transitional externally-mixed state (type 3). The κ-PDF of type 4, defined as the MH internally-mixed type, was dominated by the MH mode with a fraction larger than 70%.~~The κ-PDF of type 4 was dominated by MH mode, normally with a fraction of lager than 70%, was defined as MH internally-mixed type.~~ It should be noted that the four categories defined in our study have covered all cases of the observational results. In this study, we also calculated the standard deviation of κ-PDF (σ) according to Spitieri et al. (2023), which indicates the degree of dispersion in the data, and is

thought to reflect the mixing degree of particles to a certain extent. Given that the aerosol particles sampled at the campaign site in this study are rarely affected by other hygroscopic aerosols (e.g., aerosols from marine sources), the MH internally-mixed particles (110, 150 and 200 nm) are thus mainly from the aging and growth of smaller particles. In contrast, the larger LH internally-mixed particles are predominantly from primary emissions. Therefore, the proportion of MH and LH internally-mixed particles at 100-200 nm can be used to distinguish the contribution to the internally-mixed fraction of larger particles from smaller aerosol aging and primary emissions respectively. Specifically, the result shows that a significant proportion of the internally-mixed particles at larger size originate from the aging and growth of smaller particles, accounting for 99%, 96% and 92% respectively for 110, 150 and 200 nm particles, whereas the contribution from primary emissions to these larger internally-mixed particles is less than 10%. It is worth noting that these results may involve certain uncertainties, as the influence of other sources was not considered. For example, the more hygroscopic sulfate particles could also be directly emitted from primary sources in urban atmosphere (Dai et al., 2019); in addition, the aerosols are assumed rarely affected by the sea salts. Consequently, the contribution of smaller particle aging and growth to the internally-mixed fraction of larger particles may have been overestimated in this study. More research works are warranted to further evaluate and quantify such uncertainty in future.

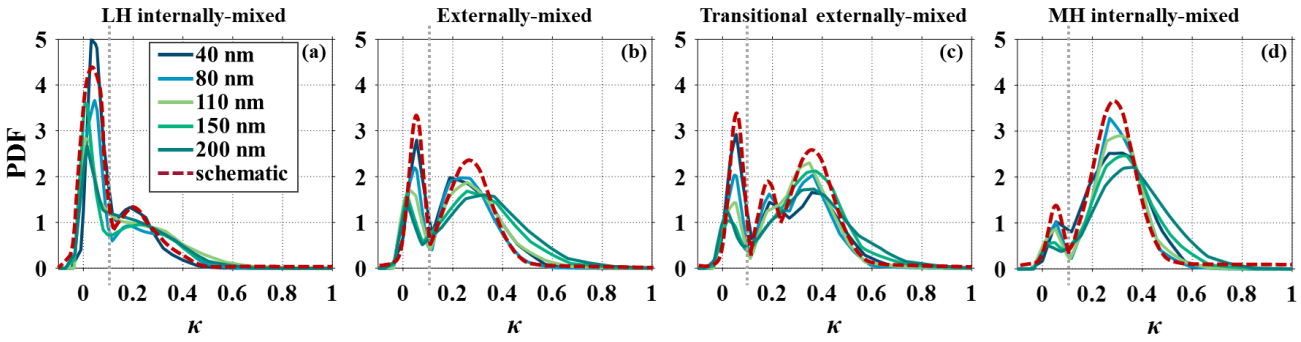

Figure 1. The mean κ-PDF of five particle sizes and the schematic diagram of κ-PDF for four mixing types.

3 Results and discussion

3.1 Overview of the mixing state of size-resolved particles

Figure 2 shows the time series of size-resolved κ, and κ versus σ. The real-time changes in the mixing states of particles are represented by different filled colors. The κ values vary from 0 to 0.5 in each of the five particle sizes, accompanied by significant changes in mixing states. In general, the mixing state of particles gradually transitions from externally-mixed to MH internally-mixed along with increases in κ. For example, particles with size of 40 nm are dominated by LH internally-mixed and externally-mixed at κ < 0.2; and the transitional externally-mixed state take up an increasingly proportion often corresponding to κ values of > 0.2 and the MH internally-mixed particles occur when κ greater than 0.3 (shown by the light gray dots in ~~Figure~~ Fig. 2).

However, there exists different correlations between κ and σ for the five sizes. For particles with diameter of 40 and 80 nm, the σ increases as the κ increases from 0.1 to 0.4 along with slight increase in the fraction of MH internally-mixed particles, showing a positive correlation. ~~While, u~~Unlike the small particles, the σ for particles larger than 100 nm (i.e., 110, 150 and 200 nm) exhibits a negative correlation to κ variations, showing that the particles were more MH internally-mixed and with stronger hygroscopicity when the smaller σ values were derived. The different sources and chemical compositions of aerosol particles could explain the distinct relationship between σ, mixing states and hygroscopicity among particles of different sizes. Here, the standard deviation of κ-PDF, σ, reflects the degree of dispersion in the pattern of κ-PDF. Taking 40 nm particles as an example, the obtained larger σ value indicates more diversity in particles hygroscopicity and chemical compositions, and thus a higher degree of external mixing state. This is because that, besides the local emissions (Ren et al., 2023), the 40 nm particles during the campaign were also from the growth of newly formed particles which are much more hygroscopic (Liu et al., 2021a). Therefore, the

composition of those small particles is more heterogeneous, resulting in both greater σ and κ. The cases where both the σ and κ of small particles are lower suggest that the particles may consist of a mixture of different species originating from primary emissions (e.g., BC, hydrocarbon-like and/or cooking organic aerosols). ~~While~~In contrast, for most of larger particles, their chemical composition tends to become homogeneous after aging and growth processes, exhibiting stronger hygroscopicity, a higher degree of internal mixing, and thus the smaller σ. However, a small number of larger particles with weak hygroscopic properties from primary emissions coexist with the aged ones in the atmosphere, which would result in larger σ and higher degree of external mixing.

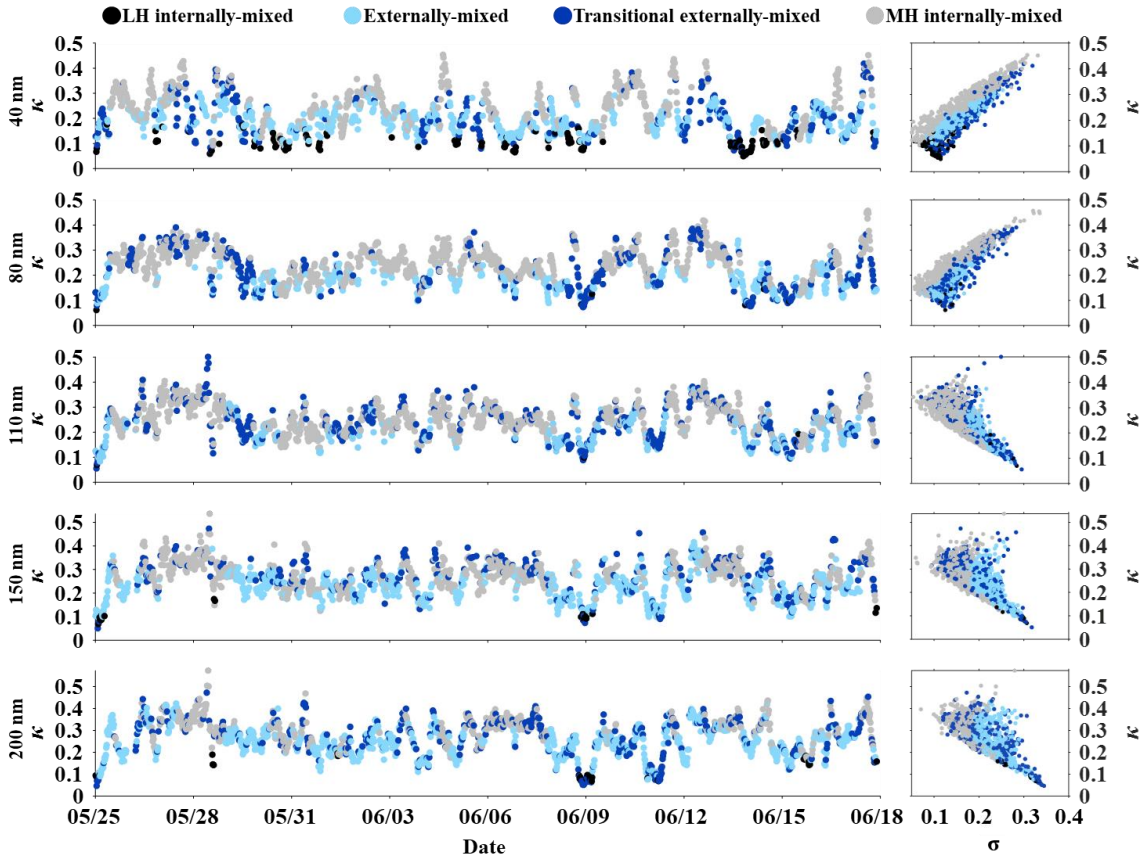

Figure 2. Time series of hygroscopic parameter (κ), and plots of κ versus standard deviation of κ-PDF (σ) for 40, 80, 110, 150 and 200 nm particles (from top to bottom). The colors denote the different mixing types.

The size dependence of mixing type fractions and σ are shown in ~~Figure~~ Fig. 3. The external mixing types, including externally-mixed and transitional externally-mixed states, dominate in 40, 150 and 200 nm particles, accounting for 53%, 57% and 70% respectively of all mixing types. The elevated fraction of externally-mixed particles is intimately associated with the local sources. For instance, a previous study revealed the particle size distribution of aerosols from different sources in urban Beijing, suggesting that the particles with diameter of 40 nm during rush hours and cooking times predominantly originated from primary emissions, and particles at 150 and 200 nm displayed a strong correlation with regional atmospheric transport sources (Ren et al., 2023). In this study, the particles exhibit weaker hygroscopicity at lower wind speeds, indicating that hydrophobic particles are primarily from local sources (~~Figure~~ Fig. S3). Furthermore, for 40 nm particles, the relatively higher fraction of MH internally-mixed particles (37%) is likely due to the growth and aging of newly formed particles (Liu et al., 2021a). This is similar to the result observed in Athens, Greece, in which the particles with 30 nm were more internally-mixed (Spitieri et al., 2023). ~~While,~~ ~~f~~For particles with sizes of 80 and 110 nm, the transitional externally-mixed and MH internally-mixed states totally account for 50-80% of all mixing types, corresponding to a significant decrease from about 10% to less than 1% of the fraction of the LH internally-mixed type. Note that the proportion of transitional externally-mixed particles remain relative constant, with a mean value of 21% across all sizes in this study, implying a continuous influence of atmospheric aging process on the particles mixing state. In addition, the larger particles (i.e., 150 nm and 200 nm) are closely associated with the growth of smaller particles and undergo a prolonged aging process. However, the fraction of MH internally-mixed

particles at 150 nm and 200 nm is lower than that of smaller particles (e.g., 80 nm and 110 nm). This is mainly due to that a considerable amount of accumulated particles observed during the campaign were emitted from primary sources, which could be externally-mixed with most of the aged more hygroscopic 150 and 200 nm aerosol particles. As shown in Fig. 3, the higher proportion of externally-mixed state was obtained for particles with diameters of 150 nm and 200 nm. Furthermore, the more active Brownian coagulation of smaller particles enhances chemical homogenization (Park et al., 2002), resulting in a much higher fraction of MH internally-mixed particles at 80 and 110 nm. ~~In addition, the 80 and 110 nm aerosols may continue aging and form 150 and 200 nm aerosol particles. Therefore, the aging of this group of aerosols should be more advanced, showing that the fraction of internally-mixed particles at 80 and 110 nm was the highest among the five particle sizes.~~ On average, the result reveals that the externally and internally mixed particles accounted for 53%±11% and 47%±11% respectively. The mixing state of particles derived in this study differs from that reported by Zhang et al. (2017), in which they conducted the measurements at a suburban site of Xinzhou, where the aerosols are much less affected by sources nearby, and the aerosols are mainly transported from elsewhere and are thus more aged and well mixed. The result implies that the influence of mixing state on hygroscopicity should be explored at specific particle sizes due to the heterogeneity of chemical compositions with particle size (Fan et al., 2020, ~~Figure~~ Fig. S4).

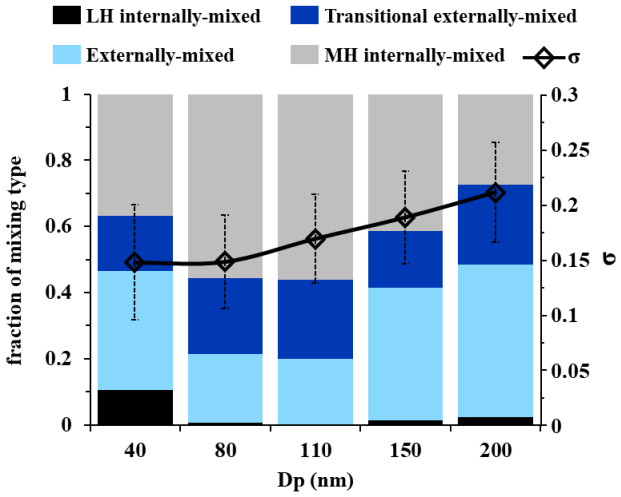

Figure 3. The size dependence of fraction of particles mixing types and σ.

Further, we compared the dependence of κ and σ on the variations of mixing states for five particle sizes (~~Figure~~ Fig. 4). At 40 and 80 nm sizes, the transition from externally-mixed to MH internally-mixed particles results in a marked increase in κ, accompanied by a slight rise in σ. ~~At 40 and 80 nm sizes, it shows that both κ and σ increases markedly when the particles change from externally-mixed to MH internally-mixed.~~ Conversely,~~While,~~ for particles with sizes of 110, 150 and 200 nm, the σ reduced but the κ increased when the particles change from externally to MH internally-mixed state. In other words, the σ of the particles larger than 80 nm shifts to lower values as the particles become more internally mixed. This contrasts with that previously observed in a vegetated site by Spitieri et al. (2023), which used only σ of Gf-PDF as a single indicator to characterize the particles mixing state. The distinct relationship between mixing type and σ for small particles (i.e., 40 and 80 nm) in urban sites indicates that the standard deviation of κ-PDF can effectively characterize mixing degree and chemical composition heterogeneity of larger particles in polluted area, where smaller aerosol particles are usually severely affected by local anthropogenic emissions.

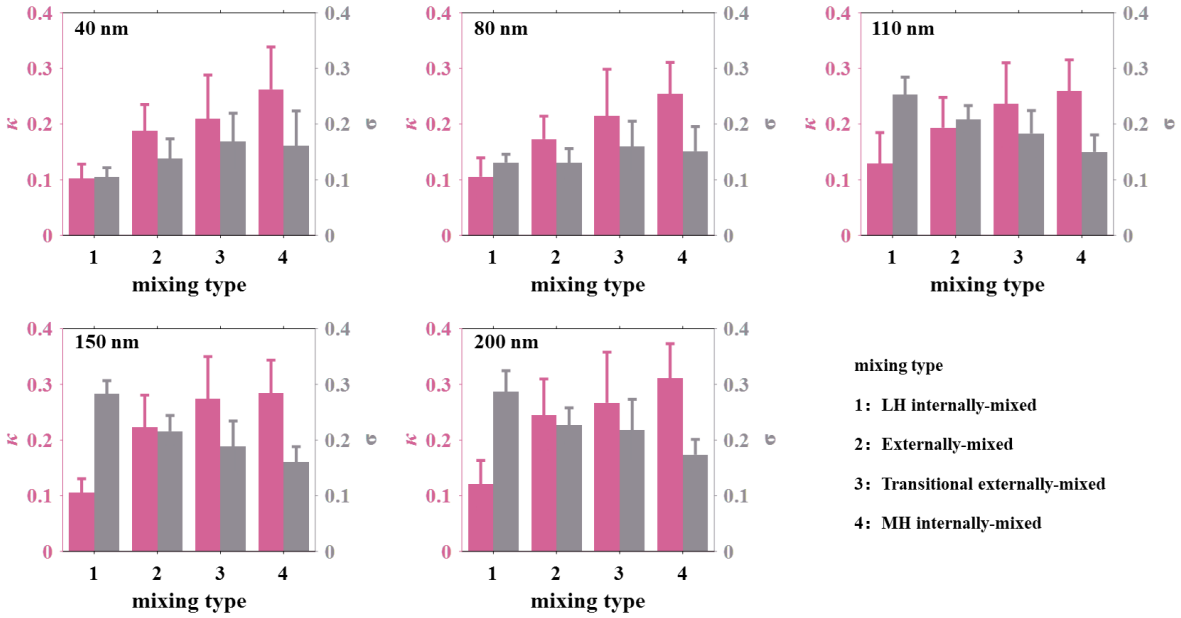

Figure 4. The mixing type dependence of hygroscopicity and σ for five particle sizes.

3.2 Evolution of mixing state of the particles

The average diurnal variations of the mixing state and κ of different particle sizes are shown in ~~Figure~~ Fig. 5. For 40 nm particles, the fraction of LH internally-mixed particles presents three peaks at morning (9:00–12:00 local time; LT), evening rush hours (18:00–20:00 LT) and nighttime (0:00–03:00 LT). This is accompanied with the impacts from those primary cooking and traffic emissions (Xu et al., 2021; Liu et al., 2021b). Unlike the 40 nm particles, there is no apparent increase of LH internally-mixed~~externally-mixed~~ state for the particles with sizes of 80, 110, 150, and 200 nm in the rush hours or cooking times. The results indicate that the particles emitted from local primary sources are small mainly with sizes around 40 nm during the campaign. Correspondingly, the proportion of the particles with MH internally-mixed state was smallest in the morning and nighttime, but exhibiting a rapid increase from about 9:00 until the evening rush hours (about 16:00–18:00). This is accompanied by the increase of hydrophobic modes in κ-PDFs of small particle sizes during rush and cooking hours measured in Beijing (~~Figure~~ Fig. S5). Moreover, the increase of externally-mixed particles of 40 nm at nighttime may be highly associated with the emissions

of primary species from heavy trucks in urban Beijing at nighttime (Hua et al., 2018), which can also be evidenced by the increased hydrophobic mode of the 150 nm and 200 nm particles observed from 00:00 to around 3:00 in ~~Figure~~ Fig. S5. In addition, the absence of photochemical aging and the lower boundary layer height during nighttime could also result in a higher proportion of externally-mixed particles. In the early afternoon, the externally-mixed and transitional externally-mixed particles, which represent the intermediate state of the aging process in which particles transition from LH to MH mode, showed a decrease to around 10%, while the proportion of particles with MH internally-mixed state increased up to 80%. ~~In addition, the externally-mixed and transitional externally-mixed particles represent the intermediate state of the aging process in which particles transition from LH to MH mode, and both showed a decrease to around 10% during the corresponding period of the day as the proportion of particles with MH internally-mixed state increased up to 80%.~~ As a result, an obvious enhancement in particles hygroscopicity was observed during the daytime, indicating the impact of particles mixing and aging on their hygroscopicity (Hersey et al., 2013; Müller et al., 2017). Overall, the diurnal variation implies an apparent aging process that leads the particles ~~changed~~ to change from externally-mixed in the early morning to MH internally-mixed in the afternoon.

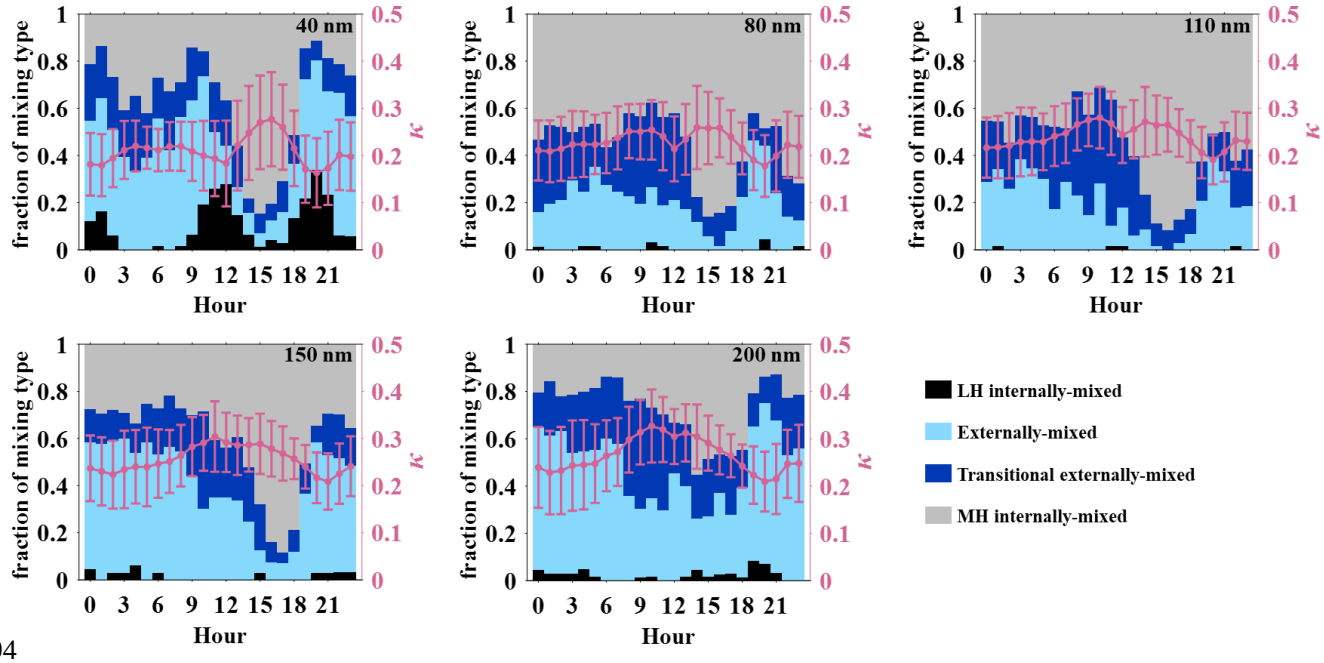

Figure 5. Diurnal variations of the mixing state fraction and κ for five particle sizes.

3.3 Particles mixing (aging) timescale: on clear and cloudy days

The aerosol particles mixing and aging process is usually accompanied by the growth of particle sizes. In order to derive the mixing and aging timescale of particles, we further analyzed the averaged diurnal variations of particles fraction with MH internally-mixed state, particle number size distributions (PNSD) and the variations of mean κ-PDF during the growth periods on both clear and cloudy days (~~Figure~~ Fig. 6). On clear days, the fraction of MH internally-mixed particles increases significantly from ~10-40% before 9:00 to ~70-100% during 12:00–15:00. ~~On clear days, the fraction of MH internally-mixed particles increases significantly from ~10-40% before 9:00 to nearly 100% during 12:00–15:00, especially for particles larger than 40 nm.~~ Such enhancement is nearly as large as that on cloudy days. In detail, the proportion of MH internally-mixed particles usually increased by less than 50% between the period before 9:00 and during 12:00–17:00, and its maximum fraction was around 50%-90%. ~~While~~In addition, the fraction of MH internally-mixed particles for 40 nm is noticeably higher on clear days (80%), which is approximately 40% greater than that on

cloudy days, indicating that photochemical processes can make particles more internally-mixed and aged (Liu et al., 2021a). Furthermore, the diurnal variations of PNSD show that the growth of particle size is highly consistent with the increase of the fraction of MH internally-mixed particles. ~~Additionally, the particles κ with large sizes at the corresponding times in the PNSD also shows an increase on both clear and cloudy days.~~ Specifically, as the particle size grows from less than 40 nm before 9:00 to ~100 nm around 17:00, the fraction of MH internally-mixed particles increases from less than 40% to >90%. And, the peak value for κ shifts from $\kappa < 0.1$ to $\kappa > 0.2$, and the count for the peak value of κ-PDF increases accordingly (~~Figure~~ Fig. 6). Overall, on clear days, the particles undergo a gradual shift from externally-mixed to MH internally-mixed states during 8:00–16:00 accompanied by a growth in particle size from 20 nm to about 100 nm, which is generally 1–2 hours shorter than that observed on cloudy days.

The obvious banana-shape growth of newly formed particles was captured in the diurnal variations of PNSD, which characterizes that the aging and growth of non-hygroscopic particles (e.g., BC) of primary emission and newly generated particles. Overall, the mixing and aging process is confirmed by the transition of particle from externally-mixed to MH internally-mixed, as well as the growth of particle size, which typically spans a duration of approximately 5 to 10 hours, as is similar to the aging timescale of aerosol particles in the polluted Indo-Gangetic Plain (< 10 hours) (Ghosh et al., 2021). In addition, the location of air parcels 5–10 hours prior to measurement was close to the sampling site in Beijing, showing that the air parcels from the northwest (cluster 5) with long-distance transport account for the least fraction (only 8%) of the air trajectories from all originating directions during the campaign (Fig. S1). This implies that most MH internally-mixed particles were formed through the aging of locally emitted externally-mixed particles. Actually, the aerosol particles aging would be largely affected by local atmospheric conditions, and thus would vary both

spatially and temporally (Pöschl et al., 2001; Huang et al., 2013). For example, using an environmental chamber approach, Peng et al. (2016) revealed that the timescale of BC aerosols aging is 2.3 and 4.6 hours, 9 and 18 hours over two cities—Beijing and Houston respectively. Note that the faster aging time in Beijing derived in the chamber experiment is probably due to the different levels in the concentration of gaseous precursors. In addition, there is only photochemical aging occurred in the chamber experiment, however, in the atmosphere, the particles aging is also through coagulation process which usually occurs slower than the photochemical reaction and condensation processes (Chen et al., 2017). This can also explain our observed faster mixing (aging) time on clear days when the photochemical process is more significant considering that the difference of the pollutant concentrations in daytime between clear and cloudy days is not obvious (i.e., O_X and PM_1; ~~Figure~~ Fig. S6).

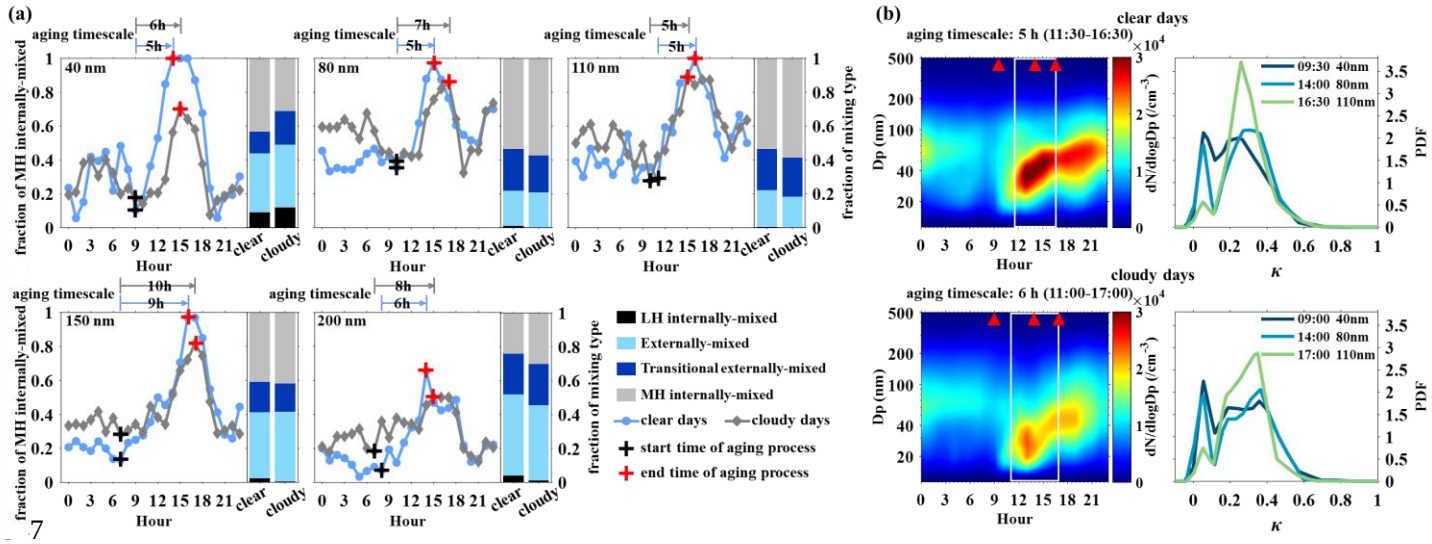

Figure 6. (a) Diurnal variations of the proportion of MH internally-mixed particles and statistical results of the fraction of mixing state for five particle sizes on clear and cloudy days. The start time of particle mixing/aging was selected when the proportion of MH internally-mixed particles is minimum between sunrise and noon, and the end time was defined as when the fraction of MH internally-mixed particles reaches its maximum. (b) The

averaged diurnal variations in PNSD and the variations of mean κ-PDF during the growth periods on clear and cloudy days (right panels). The red triangles indicate 2 hours before the start of the aging, during the growth and end of the aging process respectively.

3.4 Implications to parameterization of the current models

The mixing/aging timescale of aerosol particles significantly impacts their physiochemical properties, which in turn affects their atmospheric lifetime, transport characteristics (Zhang et al., 2023), hygroscopicity and the direct radiative forcing of aerosol particles (Moffet and Prather, 2009; Wang et al., 2018; Stevens and Dastoor, 2019). We further compared our results with the results derived from five field sites and the values adopted in current models (Table S1). In most models, the aging processes of carbonaceous aerosols were treated with a simple parameterization, which generally obtained aging time based on the transformation of aerosols from hydrophobic to hydrophilic (Chen et al., 2017; Ghosh et al., 2021). Unlike the models, the aging timescale of BC aerosols in field measurements and laboratory studies was commonly derived by tracking changes in hygroscopicity, morphology, coating thickness or optical properties (Moffet and Prather, 2009; Akagi et al., 2012; Krasowsky et al., 2016; Peng et al., 2016). These methods were used to quantify the aging timescale of particles indirectly. ~~While~~However, in our study, the mixing (aging) time was inferred based on the changes in hygroscopic modes and mixing states of non-BC particles in the ambient atmosphere. Note that although there may be some differences in the results based on different methods, the aging timescales obtained all represent the mixing and aging rate of aerosol particles in the atmosphere, which affects aerosols atmospheric lifetime, thus the environment and climate effects. As shown in ~~Figure~~ Fig. 7, the derived aging timescale of aerosols in this study is comparable to the observational results reported in other urban areas, such as Mexico City (3 hours; Moffet and Prather, 2009) and Los Angeles (3 hours; Krasowsky et al., 2016). The result is also close to the aging

timescale of particles in source area of biomass burning in California (4 hours; Akagi et al., 2012). However, the aging time of particles displays large spatial variations at different sites. For example, the aging timescale of particles observed in Beijing (4.6 hours) was four times faster than that in Houston (18 hours) where the precursors concentrations are extremely low (Peng et al., 2016). Overall, the mixing/aging timescale of particles in Beijing achieved in this study is 5–10 hours, which falls within the range of 2–10 hours in polluted areas obtained by other studies. Therefore, our results are likely representative of the aging time scale of aerosols in polluted urban areas. Furthermore, the aging time of particles obtained in ambient atmosphere is much shorter than the default values adopted in most models, which is commonly with a duration of 1.15–2.5 days. In addition, the values among different models range greatly from 1 to 20 days (~~Figure~~ Fig. 7). For example, a timescale of 20 days was used to represent a slow aging process (i.e., coagulation) by Liu et al. (2011), as may be not properly applied in regions with high particle number concentration where the particles coagulation is also efficient (Chen et al., 2017).

Although using a dynamic parameterization scheme for particles aging in models could achieve the application of different aging times to different regions, the simulated values show large variations among different models. For example, in RegCM4 model, the conversion time from fresh to aged BC ranges from about 5 hours to 7 days (Ghosh et al., 2021). The range in the KAMM/DRAIS, however, is only 2 hours to about 1.6 days (Riemer et al., 2004). Moreover, even in central-eastern China, the aging timescale has been reported to range from 12 hours to 7 days based on a regional chemical transport model (Chen et al., 2017), which is much longer than that derived in urban Beijing by this study. Additionally, the aging times of carbonaceous aerosols simulated by the GEOS-Chem model exhibit large spatial and temporal variations, with the global average calculated to be 3.1 days (Huang et

al., 2013). This value is much longer than the default values used in other global models (1-2 days) (Pierce et al., 2007). Note that although the mixing (aging) timescale of particles was determined by examining diurnal variations in the mixing state of aerosol particles in this study, compared with laboratory studies, various factors in the real ambient atmosphere change over time, including meteorological conditions, emission sources, and atmospheric processes etc. Therefore, the result derived in this study warrants further verifications. The long-term field measurements at more sites should be conducted in the future.

The large uncertainties in the aging timescale can significantly affect the accuracy of simulation and assessment for atmospheric lifetime, loading and radiation forcing of aerosols. For example, to better simulate the intercontinental transport of aerosols, Huang et al. (2013) implemented a variable aging scheme in the GEOS-Chem model, which showed that the total atmospheric burdens and global average lifetimes of BC (OC, organic carbon) were increase by 8% (2%) compared to the default value (1.15 days). Similarly, due to the implementation of the dynamic aging scheme in models, the column burden and surface mass concentration of carbonaceous aerosols increased during the dry season in the polluted Indo-Gangetic Plain, and the atmospheric heating increased by at least 1.2 W m^{-2} (Ghosh et al., 2021). Therefore, given the large spatiotemporal variations in aging timescale of particles, the study emphasizes the urgency of conducting investigations at more field sites. In addition, the other factors such as the meteorology and particle sizes that affect the aerosols aging should be accounted for so as to improve the dynamic aging schemes in climate models.

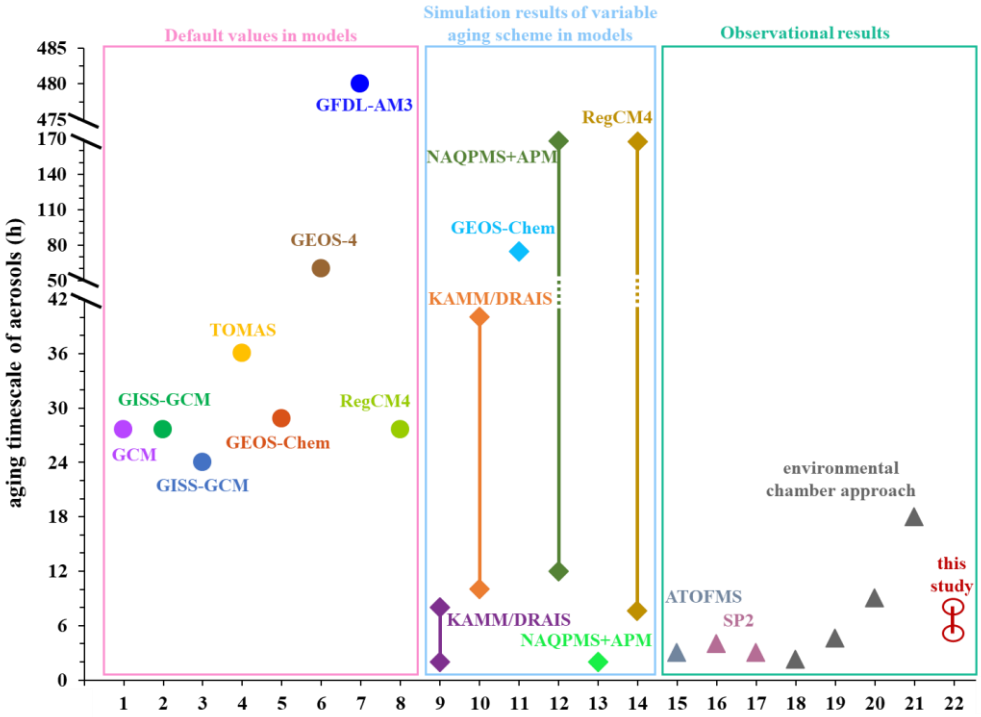

Figure 7. The mixing/aging timescale of particles reported in literatures (1. Cooke et al., 2002; 2. Chung and Seinfeld, 2002; 3. Koch and Hansen, 2005; 4. Pierce et al., 2007; 5. Yu and Luo, 2009; 6. Colarco et al., 2010; 7. Liu et al., 2011; 8, 14. Ghosh et al., 2021; 9, 10. Riemer et al., 2004; 11. Huang et al., 2013; 12, 13. Chen et al., 2017; 15. Moffet and Prather, 2009; 16. Akagi et al., 2012; 17. Krasowsky et al., 2016; 18-21. Peng et al., 2016). The solid circle, diamond and the triangle denote the default aging time of particles used in models and stimulation results of variable aging scheme in models, as well as the observational results, respectively.

4 Conclusions

The real-time mixing state of ambient aerosol particles with dry particle sizes of 40, 80, 110, 150 and 200 nm was investigated in urban Beijing, according to PDF of hygroscopic growth factor measured using the H-TDMA system. Four mixing states of ambient size-resolved particles were captured in this study. In general, particles with LH internally-mixed,

externally-mixed, transitional externally-mixed and MH internally-mixed state account for 0-10%, 20-46%, 17-24% and 27-56% respectively, which depends on particles size greatly. The fraction of MH internally-mixed particles peaks at 80 and 110 nm due to ~~enhanced~~more active Brownian coagulation enhances the chemical homogenization ~~aging in intermediate~~of particles. The diurnal variation of mixing state of particles in all sizes considered presents a visible aging process, showing that the fraction of particles with MH internally-mixed state increases significantly from ~10-40% before 9:00 to about 100% during 12:00–15:00 on clear days, accompanied by a growth in particle size from 20 nm to 100 nm. Typically, the mixing/aging process of particles takes approximately 5–10 hours, which reveals the mixing (aging) timescale of aerosols during the campaign. Additionally, our results suggest that fine aerosol particles undergo significant aging through photochemical processes in the polluted atmosphere of urban Beijing. Furthermore, there is a large difference~~the large difference of~~ in the mixing/aging timescale of particles between values in models and the timescale achieved by observations, emphasizing the vital role of exploring the aging timescale through more field measurements to improve the accuracy of aging schemes in climate models. The results revealed in our study highlight the considerable impact of atmospheric aging on mixing state of fine aerosol particles in polluted megacities.

Data availability

All data used in the study are available from the corresponding author upon request (zhangfang2021@hit.edu.cn).

Author contributions

FZ and JL conceived the conceptual development of the paper. FZ, JR, LC and JL directed and performed of the experiments with AZ, ZW, SZ, HX and XY. JL conducted the data analysis and wrote the draft. All authors edited and commented on the various sections of the paper.

Competing interests

The authors declare that they have no conflict of interest.

Acknowledgments

This work was funded by the National Natural Science Foundation of China (NSFC) research project (Grant No. 42475112, 42405191), Shenzhen Science and Technology Plan Project (Grant No. GXWD20220811174022002; KCXST20221021111404011), Guangdong Natural Science Foundation (Grant No. 2024A1515011005), Hebei Natural Science Foundation (Grant No. D2024205006). We thank all participants in the field campaigns for their tireless work and cooperation.

Reference

Akagi, S. K., Craven, J. S., Taylor, J. W., McMeeking, G. R., Yokelson, R. J., Burling, I. R., Urbanski, S. P., Wold, C. E., Seinfeld, J. H., Coe, H., Alvarado, M. J., and Weise, D. R.: Evolution of trace gases and particles emitted by a chaparral fire in California, Atmos. Chem. Phys., 12, 1397–1421, https://doi.org/10.5194/acp-12-1397-2012, 2012.

Chen, L., Zhang, F., Yan, P., Wang, X., Sun, L., Li, Y., Zhang, X., Sun, Y., and Li, Z.: The large proportion of black carbon (BC)-containing aerosols in the urban atmosphere,

Environ. Pollut., 263, Part B, https://doi.org/10.1016/j.envpol.2020.114507, 2020.

Chen, L., Zhang, F., Zhang, D., Wang, X., Song, W., Liu, J., Ren, J., Jiang, S., Li, X., and Li, Z.: Measurement report: Hygroscopic growth of ambient fine particles measured at five sites in China, Atmos. Chem. Phys., 22, 6773–6786, https://doi.org/10.5194/acp-22-6773-2022, 2022.

Chen, X., Wang, Z., Yu, F., Pan, X., Li, J., Ge, B., Wang, Z., Hu, M., Yang, W., and Chen, H.: Estimation of atmospheric aging time of black carbon particles in the polluted atmosphere over central-eastern China using microphysical process analysis in regional chemical transport model, Atmos. Environ., 163, 44–56, https://doi.org/10.1016/j.atmosenv.2017.05.016, 2017.

Chung, S., and Seinfeld, J.: Global distribution and climate forcing of carbonaceous aerosols, J. Geophys. Res.-Atmos., 107(D19), 4407, https://doi.org/10.1029/2001JD001397, 2002.

Colarco, P., Silva, A., Chin, M., and Diehl, T.: Online simulations of global aerosol distributions in the NASA GEOS-4 model and comparisons to satellite and ground-based aerosol optical depth, J. Geophys. Res.-Atmos., 115, D14207, https://doi.org/10.1029/2009JD012820, 2010.

Cooke, W., Ramaswamy, V., and Kasibhatla, P.: A general circulation model study of the global carbonaceous aerosol distribution, J. Geophys. Res.-Atmos., 107(D16), https://doi.org/10.1029/2001JD001274, 2002.

Dai, Q., Bi, X., Song, W., Li, T., Liu, B., Ding, J., Xua, J., Song, C., Yang, N., Schulze, B.C., Zhang, Y., Feng, Y., and Hopke, P.K.: Residential coal combustion as a source of primary sulfate in Xi'an, China, Atmos. Environ., 196, 66–76,

https://doi.org/10.1016/j.atmosenv.2018.10.002, 2019.

Enroth, J., Mikkilä, J., Németh, Z., Kulmala, M., and Salma, I.: Wintertime hygroscopicity and volatility of ambient urban aerosol particles, Atmos. Chem. Phys., 18, 4533–4548, https://doi.org/10.5194/acp-18-4533-2018, 2018.

Fan, X., Liu, J., Zhang, F., Chen, L., Collins, D., Xu, W., Jin, X., Ren, J., Wang, Y., Wu, H., Li, S., Sun, Y., and Li, Z.: Contrasting size-resolved hygroscopicity of fine particles derived by HTDMA and HR-ToF-AMS measurements between summer and winter in Beijing: the impacts of aerosol aging and local emissions, Atmos. Chem. Phys., 20, 915–929, https://doi.org/10.5194/acp-20-915-2020, 2020.

Ge, S., Su, J., Zhao, P., Li, J., Liu, S., Qiu, Y., Pu, W., and Ma, Z.: Characteristics of $PM_{2.5}$ hygroscopicity and the influences of water-soluble ions during haze events in Beijing, Atmos. Environ., 120382, https://doi.org/10.1016/j.atmosenv.2024.120382, 2024.

Ghosh, S., Riemer, N., Giuliani, G., Giorgi, F., Ganguly, D., and Dey, S.: Sensitivity of carbonaceous aerosol properties to the implementation of a dynamic aging parameterization in the regional climate model RegCM, J. Geophys. Res.-Atmos., 126, https://doi.org/10.1029/2020JD033613, 2021.

Gysel, M., McFiggans, G. B., and Coe, H.: Inversion of tandem differential mobility analyser (TDMA) measurements, J. Aerosol Sci., 40, 134–151, https://doi.org/10.1016/j.jaerosci.2008.07.013, 2009.

Hersey, S. P., Craven, J. S., Metcalf, A. R., Lin, J., Lathem, T., Suski, K., Cahill, J., Duong, H., Sorooshian, A., Jonsson, H., Shiraiwa, M., Zuend, A., Nenes, A., Prather, K., Flagan, R., and Seinfeld, J.: Composition and hygroscopicity of the los angeles aerosol: CalNex,

J. Geophys. Res.-Atmos., 118(7): 3016-3036, https://doi.org/10.1002/jgrd.50307, 2013.

Hong, J., Xu, H., Tan, H., Yin, C., Hao, L., Li, F., Cai, M., Deng, X., Wang, N., Su, H., Cheng, Y., Wang, L., Petäjä, T., and Kerminen, V.-M.: Mixing state and particle hygroscopicity of organic-dominated aerosols over the Pearl River Delta region in China, Atmos. Chem. Phys., 18, 14079–14094, https://doi.org/10.5194/acp-18-14079-2018, 2018.

Hua, Y., Wang, S., Jiang, J., Zhou, W., Xu, Q., Li, X., Liu, B., Zhang, D., and Zheng, M.: Characteristics and sources of aerosol pollution at a polluted rural site southwest in Beijing, China, Sci. Total Environ., 626, 519-527, https://doi.org/10.1016/j.scitotenv.2018.01.047, 2018.

Huang, Y., Wu, S., Dubey, M. K., and French, N. H. F.: Impact of aging mechanism on model simulated carbonaceous aerosols, Atmos. Chem. Phys., 13, 6329–6343, https://doi.org/10.5194/acp-13-6329-2013, 2013.

Jacobson, M.: Strong radiative heating due to the mixing state of black carbon in atmospheric aerosols, Nature, 409, 695–697, https://doi.org/10.1038/35055518, 2001.

Koch, D., Hansen, J.: Distant origins of Arctic black carbon: A Goddard Institute for Space Studies Model experiment, J. Geophys. Res.-Atmos., 110, D04204, https://doi.org/10.1029/2004JD005296, 2005.

Krasowsky, T., McMeeking, G., Wang, D., Sioutas, C., Ban-Weiss, G.: Measurements of the impact of atmospheric aging on physical and optical properties of ambient black carbon particles in Los Angeles, Atmos. Environ., 142, 496-504, https://doi.org/10.1016/j.atmosenv.2016.08.010, 2016.

Liu, D., Joshi, R., Wang, J., Yu, C., Allan, J. D., Coe, H., Flynn, M. J., Xie, C., Lee, J.,

Squires, F., Kotthaus, S., Grimmond, S., Ge, X., Sun, Y., and Fu, P.: Contrasting physical properties of black carbon in urban Beijing between winter and summer, Atmos. Chem. Phys., 19, 6749–6769, https://doi.org/10.5194/acp-19-6749-2019, 2019.

Liu, J., Fan, S., Horowitz, L., and Levy II, H.: Evaluation of factors controlling long-range transport of black carbon to the Arctic, J. Geophys. Res.-Atmos., 116, D04307, https://doi.org/10.1029/2010JD015145, 2011.

Liu, J., Zhang, F., Xu, W., Sun, Y., Chen, L., Li, S., Ren, J., Hu, B., Wu, H., and Zhang, R.: Hygroscopicity of organic aerosols linked to formation mechanisms, Geophys. Res. Lett., 48, e2020GL091683, https://doi.org/10.1029/2020GL091683, 2021a.

Liu, J., Zhang, F., Xu, W., Chen, L., Ren, J., Jiang, S., Sun, Y., and Li, Z.: A large impact of cooking organic aerosol (COA) on particle hygroscopicity and CCN activity in urban atmosphere, J. Geophys. Res.-Atmos., 126, e2020JD033628, https://doi.org/10.1029/2020JD033628, 2021b.

Li, S., Zhang, F., Jin, X., Sun, Y., Wu, H., Xie, C., Chen, L., Liu, J., Wu, T., Jiang, S., Maureen, C., and Li, Z.: Characterizing the ratio of nitrate to sulfate in ambient fine particles of urban Beijing during 2018–2019, Atmos. Environ., 237, https://doi.org/10.1016/j.atmosenv.2020.117662, 2020.

Li, W., Sun, J., Xu, L., Shi, Z., Riemer, N., Sun, Y., Fu, P., Zhang, J., Lin, Y., Wang, X., Shao, L., Chen, J., Zhang, X., Wang, Z., and Wang W.: A conceptual framework for mixing structures in individual aerosol particles, J. Geophys. Res.-Atmos., 121(22), 13784-13798, https://doi.org/10.1002/2016JD025252, 2016.

Moffet, R., and Prather, K.: In-situ measurements of the mixing state and optical properties of

soot with implications for radiative forcing estimates, P. Natl. Acad. Sci. USA, 106(29), 11872-11877, https://doi.org/10.1073/pnas.0900040106, 2009.

Müller, A., Miyazaki, Y., Aggarwal, S., Kitamori, Y., Boreddy, S., and Kawamura, K.: Effects of chemical composition and mixing state on size-resolved hygroscopicity and cloud condensation nuclei activity of submicron aerosols at a suburban site in northern Japan in summer, J. Geophys. Res.-Atmos., 122(17), 9301-9318, https://doi.org/10.1002/2017JD027286, 2017.

Park, S. H., Kruis, F. E., Lee, K. W., and Fissan, H.: Evolution of Particle Size Distributions due to Turbulent and Brownian Coagulation, Aerosol Sci. Technol., 36(4), 419-432, https://doi.org/10.1080/027868202753571241, 2002.

Peng, J. F., Hu, M., Guo, S., Du, Z. F., Zheng, J., Shang, D. J., Zamora, M., Zeng, L. M., Shao, M., Wu, Y. S., Zheng, J., Wang, Y., Glen, C., Collins, D., Molina, M., and Zhang, R. Y.: Markedly enhanced absorption, and direct radiative forcing of black carbon under polluted urban environments, P. Natl. Acad. Sci. USA, 113, 4266–4271, https://doi.org/10.1073/pnas.1602310113, 2016.

Petters, M. D. and Kreidenweis, S. M.: A single parameter representation of hygroscopic growth and cloud condensation nucleus activity, Atmos. Chem. Phys., 7, 1961–1971, https://doi.org/10.5194/acp-7-1961-2007, 2007.

Pierce, J. R., Chen, K., and Adams, P. J.: Contribution of primary carbonaceous aerosol to cloud condensation nuclei: processes and uncertainties evaluated with a global aerosol microphysics model, Atmos. Chem. Phys., 7, 5447–5466, https://doi.org/10.5194/acp-7-5447-2007, 2007.

Pöschl, U., Letzel, T., Schauer, C., and Niessner, R.: Interaction of ozone and water vapor with spark discharge soot aerosol particles coated with benzo[a]pyrene : O_3 and H_2O adsorption, benzo[a]pyrene degradation, and atmospheric implications, J. Phys. Chem. A, 16, 105, https://doi.org/10.1021/jp004137n, 2001.

Ren, J., Zhang, F., Wang, Y., Collins, D., Fan, X., Jin, X., Xu, W., Sun, Y., Cribb, M., and Li, Z.: Using different assumptions of aerosol mixing state and chemical composition to predict CCN concentrations based on field measurements in urban Beijing, Atmos. Chem. Phys., 18, 6907–6921, https://doi.org/10.5194/acp-18-6907-2018, 2018.

Ren, J., Zhang, F., Chen, L., Cao, G., Liu, M., Li, X., Wu, H., Cheng, Y., and Li, Z.: Identifying the hygroscopic properties of fine aerosol particles from diverse sources in urban atmosphere and the applicability in prediction of cloud nuclei, Atmos. Environ., 298, 119615, https://doi.org/10.1016/j.atmosenv.2023.119615, 2023.

Riemer, N., Vogel, H., and Vogel, B.: Soot aging time scales in polluted regions during day and night, Atmos. Chem. Phys., 4, 1885–1893, https://doi.org/10.5194/acp-4-1885-2004, 2004.

Riemer, N., Ault, A. P., West, M., Craig, R. L., and Curtis, J. H.: Aerosol mixing state: Measurements, modeling, and impacts, Rev. Geophys., 57, 187–249, https://doi.org/10.1029/2018RG000615, 2019.

Saha, P. K., Khlystov, A., and Grieshop, A. P.: Downwind evolution of the volatility and mixing state of near-road aerosols near a US interstate highway, Atmos. Chem. Phys., 18, 2139–2154, https://doi.org/10.5194/acp-18-2139-2018, 2018.

Shi, J., Hong, J., Ma, N., Luo, Q., He, Y., Xu, H., Tan, H., Wang, Q., Tao, J., Zhou, Y., Han, S.,

611 Peng, L., Xie, L., Zhou, G., Xu, W., Sun, Y., Cheng, Y., and Su, H.: Measurement report:
612 On the difference in aerosol hygroscopicity between high and low relative humidity
613 conditions in the North China Plain, Atmos. Chem. Phys., 22, 4599–4613,
614 https://doi.org/10.5194/acp-22-4599-2022, 2022.
615 Spitieri, C., Gini, M., Gysel-Beer, M., and Eleftheriadis, K.: Annual cycle of hygroscopic
616 properties and mixing state of the suburban aerosol in Athens, Greece, Atmos. Chem.
617 Phys., 23, 235-249, https://doi.org/10.5194/acp-23-235-2023, 2023.
618 Stevens, R., and Dastoor, A.: A Review of the Representation of Aerosol Mixing State in
619 Atmospheric Models, Atmos., 10(4), 168, https://doi.org/10.3390/atmos10040168, 2019.
620 Sun, Y. L., Wang, Z. F., Du, W., Zhang, Q., Wang, Q. Q., Fu, P. Q., Pan, X. L., Li, J., Jayne, J.,
621 and Worsnop, D. R.: Longterm real-time measurements of aerosol particle composition
622 in Beijing, China: seasonal variations, meteorological effects, and source analysis,
623 Atmos. Chem. Phys., 15, 10149–10165, https://doi.org/10.5194/acp-15-10149-2015,
624 2015.
625 Swietlicki, E., Hansson, H. C., Hameri, K., Svenningsson, B., Massling, A., Mcfiggans, G., P.
626 Mcmurry, H., Petäjä, T., Tunved, P., Gysel, M., Topping, D., Weingartner, E.,
627 Baltensperger, U., Rissler, J., Wiedensohler, A., and Kulmala, M.: Hygroscopic
628 properties of submicrometer atmospheric aerosol particles measured with H-TDMA
629 instruments in various environments - a review, Tellus B, 60(3), 432–469,
630 https://doi.org/10.1111/j.1600-0889.2008.00350.x, 2008.
631 Wang, Y., Li, Z., Zhang, R., Jin, X., Xu, W., Fan, X., Wu, H., Zhang, F., Sun, Y., and Wang,
632 Q.: Distinct ultrafine- and accumulation-mode particle properties in clean and polluted

633 urban environments, Geophys. Res. Lett., 46, 10,918–10,925,
634 https://doi.org/10.1029/2019GL084047, 2019.
635 Wang, Y., Ma, P.-L., Peng, J., Zhang, R., Jiang, J. H., Easter, R. C., and Yung, Y. L.:
636 Constraining aging processes of black carbon in the Community Atmosphere Model
637 using environmental chamber measurements, J. Adv. Model. Earth Sy., 10, 2514–2526.
638 https://doi.org/10.1029/2018MS001387, 2018.
639 Wang, Z., Shi, C., Zhang, H., Chen, Y., Chi, X., Xia, C., Wang, S., Zhu, Y., Zhang, K., Chen,
640 X., Xing, C., and Liu, C.: Measurement report: Dust and anthropogenic aerosols' vertical
641 distributions over northern China dense aerosols gathered at the top of the mixing layer,
642 Atmos. Chem. Phys., 23, 14271–14292, https://doi.org/10.5194/acp-23-14271-2023,
643 2023.
644 Winkler, P.: The growth of atmospheric aerosol particles as a function of the relative
645 humidity—II. An improved concept of mixed nuclei, J. Aerosol Sci., 4(5), 373–387,
646 https://doi.org/10.1016/0021-8502(73)90027-X, 1973.
647 Xie, C., He, Y., Lei, L., Zhou, W., Liu, J., Wang, Q., Xu, W., Qiu, Y., Zhao, J., Sun, J., Li, L.,
648 Li, M., Zhou, Z., Fu, P., Wang, Z., and Sun, Y.: Contrasting mixing state of black
649 carbon-containing particles in summer and winter in Beijing, Environ. Pollut., 263,
650 114455, https://doi.org/10.1016/j.envpol.2020.114455, 2020.
651 Xu, W., Chen, C., Qiu, Y., Xie, C., Chen,Y., Ma, N., Xu, W., Fu, P., Wang, Z., and Pan, X.:
652 Size-resolved characterization of organic aerosol in the North China Plain: new insights
653 from high resolution spectral analysis, Environ. Sci.: Atmos., 1(6), 346–358,
654 https://doi.org/10.1039/D1EA00025J, 2021.

Xu, W., Xie, C., Karnezi, E., Zhang, Q., Wang, J., Pandis, S. N., Ge, X., Zhang, J., An, J., Wang, Q., Zhao, J., Du, W., Qiu, Y., Zhou, W., He, Y., Li, Y., Li, J., Fu, P., Wang, Z., Worsnop, D. R., and Sun, Y.: Summertime aerosol volatility measurements in Beijing, China, Atmos. Chem. Phys., 19, 10205–10216, https://doi.org/10.5194/acp-19-10205-2019, 2019.

Yao, Y., Curtis, J. H., Ching, J., Zheng, Z., and Riemer, N.: Quantifying the effects of mixing state on aerosol optical properties, Atmos. Chem. Phys., 22, 9265–9282, https://doi.org/10.5194/acp-22-9265-2022, 2022.

Yu, F. and Luo, G.: Simulation of particle size distribution with a global aerosol model: contribution of nucleation to aerosol and CCN number concentrations, Atmos. Chem. Phys., 9, 7691–7710, https://doi.org/10.5194/acp-9-7691-2009, 2009.

Zhang, F., Wang, Y., Peng, J., Ren, J., Collins, D., Zhang, R., Sun, Y., Yang, X., and Li, Z.: Uncertainty in Predicting CCN Activity of Aged and Primary Aerosols, J. Geophys. Res.-Atmos., 122, 11723–11736, https://doi.org/10.1002/2017JD027058, 2017.

Zhang, J., Li, W., Wang, Y., Teng, X., Zhang, Y., Xu, L., Yuan, Q., Wu, G., Niu, H., and Shao, L.: Structural collapse and coating composition changes of soot particles during long-range transport, J. Geophys. Res.-Atmos., 128, e2023JD038871, https://doi.org/10.1029/2023JD038871, 2023.